Enhanced FDG-PET Tumor Imaging with Correlation-Coefficient Filtered Influx-Constant Images

Kenneth R. Zasadny and Richard L. Wahl
Department of Internal Medicine, Division of Nuclear Medicine, University of Michigan Medical Center, Ann Arbor, Michigan

Although FDG is an excellent PET tumor imaging agent, residual tracer activity in normal structures such as blood vessels and the liver can impair the detection of small or modestly tracer-avid tumors. Since tumors generally have a continuous influx of FDG over time while normal tissues generally show tracer efflux, we produced and optimized correlation-coefficient constrained influx-constant "parametric" images to maximize tumor visualization but minimize background and artifacts for FDG-PET cancer imaging. **Methods:** Influx-constant image sets were generated in 17 patients with various cancers for a range of correlation-coefficient constraint values. Quantitative evaluation of the parametric PET images was performed. **Results:** Image noise was reduced 70% (mean) with no loss of tumor signal for $r \geq 0.90$ constraint versus no constraint. Higher (0.95–0.99) constraints improved tumor-to-normal ratios but resulted in some loss of tumor signal. Mild constraints (0–0.85) produced more background artifacts than higher constraints, though all correlation constraints improved tumor-to-normal ratios over the single 50–60-min acquisition frame. **Conclusion:** Correlation-coefficient filtered parametric imaging, especially with an r-value constraint of ≥0.90, enhances tumor-to-normal contrast for FDG-PET and appears promising for improving lesion detectability.

Key Words: PET; emission computed tomography; flurodeoxyglucose; tumor imaging; cancer

J Nucl Med 1996; 37:371–374

Previous efforts have shown that pixel-by-pixel parametric images can be generated to reflect myocardial and brain glucose metabolism (i.e., tracer influx) as estimated by PET (*1*). Images are generally high quality because of the avid influx of FDG into myocardium and brain. Furthermore, input functions necessary for parametric images have been shown to be valid when derived directly from a region of interest (ROI) drawn in the left ventricle or a great vessel (*1–5*), thus leading to quantitative images derived solely from a noninvasive imaging method. We exploit this noninvasive procedure for the generation of parametric images of cancer using FDG and an image-derived input function. Messa et al. (*6*) have shown preliminary data for metabolic images of liver metastases in a limited number of patients.

The motivation for our work is to improve the tumor-to-normal tissue PET image signal, since even after 60 min post-FDG injection, there is substantial blood-born activity remaining, possibly impairing the ability to detect small tumor foci near blood vessels, or in or near structures with high normal ^{18}F activity. Indeed, the normal lean body mass-corrected standardized uptake value of blood is 1.7 and 2.0 for liver at 1 hr post-FDG injection (*7*). While PET is a sensitive method and superior to CT scanning in staging lung cancer, our recent prospective study of lung cancer staging showed nearly a 20% false-negative rate in mediastinal lymph node staging (*8*), although residual blood-pool FDG activity may be contributing to this finding. Figure 1 shows time-activity curves for tumor and normal tissues in 18 patients with untreated primary breast cancers. Note that FDG accumulation in tumors tends to rise with time, while accumulation in most normal tissues imaged decreased, with the possible exception of marrow in these fasting patients. We have preliminary findings that this pattern is true in at least 80% of untreated primary cancers (*9,10*).

The tissue concentration of ^{18}F activity can be expressed as (*11*):

$$C_T(t) = K_i \int_0^t C_p(s)ds + V(t)C_p(t),\ K_i = \frac{K_1k_3}{k_2 + k_3}. \quad \text{Eq. 1}$$

The rate of glucose metabolism in tissue can be expressed as:

$$MR_T = \left(\frac{C_p}{LC}\right)\left(\frac{K_1k_3}{k_2 + k_3}\right) = \left(\frac{C_p}{LC}\right)K_i, \quad \text{Eq. 2}$$

where C_p is the plasma concentration of ^{18}F activity and LC is the lumped constant relating FDG metabolism to glucose metabolism. K_1, k_2 and k_3 are rate parameters of FDG flow from plasma to tissue (K_1), flow from tissue back to plasma (k_2) and phosphorylation rate to FDG-6 phosphate (k_3). This model assumes a negligible rate for dephosphorylation of FDG-6 phosphate, i.e., $k_4 = 0$. Investigations confirm that for most untreated tumors, k_4 is a very small quantity (*12*). Also, it has been shown that levels of phosphatase in many tumors are near zero, implying that k_4 can generally be neglected (*12*). Normal tissues that contain significant levels of phosphatase (i.e., liver and kidney) will not be properly modeled by neglecting k_4, though this assumption (i.e., that $k_4 = 0$) will underestimate the value of K_i for these tissues, thus further increasing the tumor-to-normal tissue ratio, as shown by Messa et al. (*6*), for liver metastases in relation to normal liver. The lumped constant in tumors is not yet fully defined, however, so the metabolic rate is viewed as an estimate only.

Pixel-by-pixel analysis of $C_T(t)/C_p(t)$ versus $\int_0^t C_p(s)ds/C_p(t)$ can produce noisy influx images, because of low count rates in some tissues (*9*). Emission images containing streak artifacts that can lead to significant slope values because of the persistence of the streaks throughout the dynamic imaging sequence also contribute to K_i image noise. Noisy K_i images complicate the tumor detection problem because of the persistence of image streak artifacts, even though normal tissue and blood levels are reduced. Figure 2 shows that there is a qualitative improvement

Received Nov. 29, 1994; revision accepted Jun. 7, 1995.
For correspondence or reprints contact: Richard L. Wahl, MD, Division of Nuclear Medicine, University of Michigan Medical Center, 1500 E. Medical Center Dr., B1G412, Ann Arbor, MI 48109-0028.

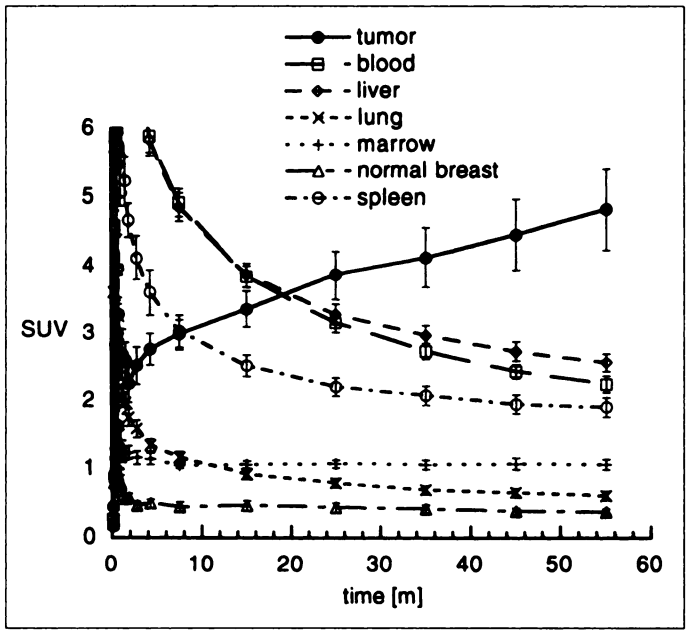

FIGURE 1. Mean time-activity curves (± s.e.m.) for tumor and normal tissues in 18 women with untreated primary breast cancer. On average, tumor activity increased as a function of time relative to blood and normal tissues through 60 min.

in tumor visualization relative to blood and liver in the K_i image (input function derived from left atrium) versus a 50–60-min post-FDG injection frame, but image noise artifacts remain.

The simple linear approach of the Patlak-Gjedde model makes estimation of the influx constant slope on a pixel-by-pixel basis quite practical. The K_i-slope image is a one-parameter approach to improve image contrast over static imaging, namely that tumor would have a higher influx and retention of FDG over most other normal tissues as a function of time. One could hypothesize that a further improvement in influx-image quality could result if one also considers the quality of the Patlak model fit as a second parameter. This approach assumes that tumor tissue would not only produce higher K_i slope values over normal tissues, but also result in a better fit over other normal tissues, specifically image noise artifacts. The correlation coefficient for a weighted-linear least squares fit is defined as (*13*):

$$r = \frac{\sum_i w_i \sum_i w_i x_i y_i - \sum_i w_i x_i \sum_i w_i y_i}{\sqrt{\left[\sum_i w_i \sum_i w_i x_i^2 - \left(\sum_i w_i x_i\right)^2\right]\left[\sum_i w_i \sum_i w_i y_i^2 - \left(\sum_i w_i y_i\right)^2\right]}},$$

where $x_i = \int_0^t C_p(s)ds/C_p(t_i)$ and $y_i = C_T(t_i)/C_p(t_i)$. The weights, w_i, are estimates of the variance of the counts per pixel and are assumed to be $1/C_T(t_i)$. Evaluation of the r-function for each pixel adds little computation time to the slope image analysis. The appropriate level of correlation-coefficient filtering would have to be empirically determined in order to investigate the range of values that produce the best tumor-to-normal tissue and tumor-to-noise contrast ratios. Also of importance is the effect of correlation-coefficient filtering on the tumor signal itself. In this report we quantitatively compared correlation coefficient filtered images of differing correlation coefficient values to determine the potential of this image enhancement approach.

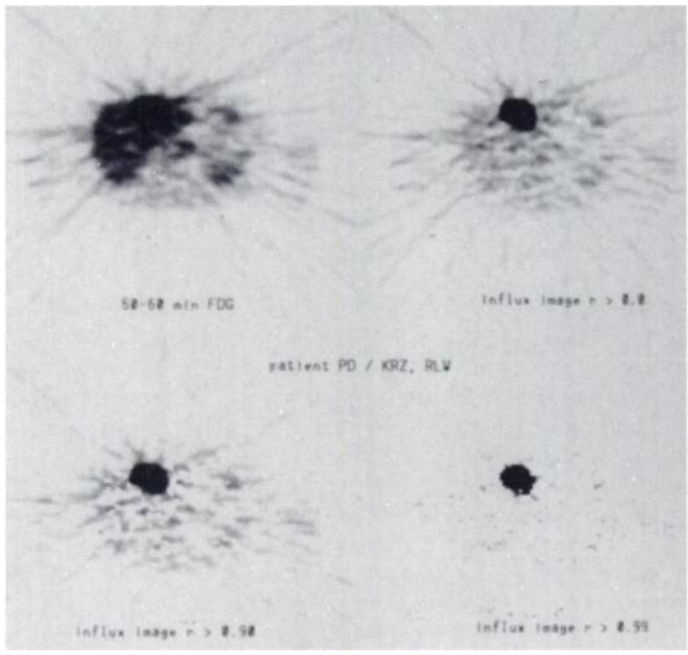

FIGURE 2. A 50–60-min static image, influx image with no correlation constraint, influx image with $r \geq 0.90$ constraint and influx image with $r \geq 0.99$ constraint in a patient with metastatic breast cancer (left atrium input function). Note reduction in normal liver activity in the influx constant images, enhancing tumor visualization.

MATERIALS AND METHODS

Seventeen patients with a variety of cancers were studied with FDG-PET: five breast cancers, two colon cancers, seven lung cancers, one lymphoma, one ovarian cancer and one renal cancer. Patients were studied as a part of several ongoing clinical studies of the efficacy of PET imaging of cancer. All patients provided written informed consent for their PET studies. Attenuation correction of the reconstructed images was accomplished by acquiring a patient-specific transmission study using a ^{68}Ge ring source. Dynamic images were acquired with a Siemens 931ECAT or 921EXACT camera (Siemens, Des Plaines, IL) with a 10-cm or 16-cm transaxial field of view, respectively. Seventeen dynamic data frames were acquired for 1 hr after intravenous injection of approximately 370 MBq FDG intravenously—6 × 10 sec, 3 × 20 sec, 2 × 90 sec, 1 × 300 sec, 5 × 600 sec. Images were reconstructed with a Hanning-filtered backprojection algorithm with a 0.3 cutoff value.

The input function curve, $C_p(t)$, was derived from a ROI in the left atrium for images including the left atrium. In cases where the heart was not in the field of view, an estimate (though a systematic underestimate due to count losses from the partial-volume effect) of the input function was generated from an ROI placed around descending aorta or femoral arteries. Corrections for partial count recovery were not made; however, the contrast-enhancing effect of the K_i analysis will not be affected since the general shape of the input function is maintained, though the absolute value of K_i will be overestimated because of the underestimate of $C_p(t)$. Images were fitted to the Patlak analysis for dynamic time points from 5 to 60 min (last six frames of data) for correlation-constraint filter values of $r \geq 0$, 0.75, 0.80, 0.85, 0.90, 0.95, 0.98 and 0.99 on a pixel-by-pixel basis, setting pixel values to zero that did not meet the minimum correlation-coefficient constraint. A single correlation coefficient filtered image set for 47 planes of data required approximately 5 min of processing time on a VAXstation 3520 (Digital Equipment Corp., Maynard, MA). ROIs were drawn around the tumor perimeter (as determined visually) in the slice containing the maximum tumor diameter for the 17 patients studied

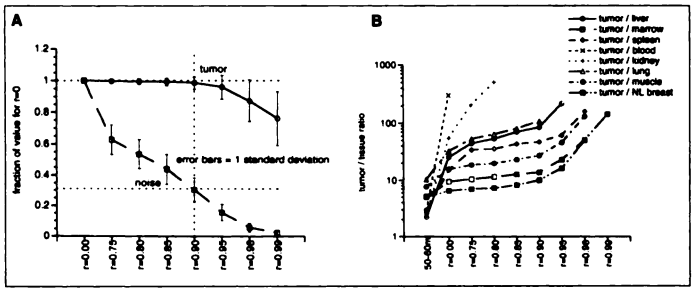

FIGURE 3. (A) Tumor and background noise signal as a percent of basal value (either 50–60-min static or $r \geq 0$ for influx images). There is a rapid loss of noise signal for a modest correlation constraint value of $r \geq 0.75$, with no adverse affect on tumor signal. (B) Tumor-to-normal tissue ratios as a function of increasing correlation constraint value. Also note that even when there is degradation in tumor signal for higher constraint values ($r > 0.90$), the tumor-to-normal tissue contrast still increases.

to investigate the effect of r-value filtering on tumor signal. ROIs were also placed on normal tissues and blood in the field of view, including a large ROI placed outside the patient boundary to quantitate image streak artifacts and noise. The quantitative determinations of tumor and background signal from the various datasets were then compared.

RESULTS

Figure 2 shows images (50–60-min static, influx images for $r \geq 0$, 0.90 and 0.99) for a patient with metastatic breast cancer involving the liver. Influx constant images show improvement in tumor-to-normal tissue signal relative to the 50–60-min static image, and increasing r-value filtering of the influx constant images shows further improvement in tumor-to-normal tissue and tumor-to-noise ratios with little effect on tumor signal. Similar images in patients with lung cancer show decreased blood activity background in the influx images compared to the 50–60-min static acquisition. Normal kidney signal is eliminated in influx images of the abdomen.

Figure 3A shows the mean tumor signal intensity and mean noise level outside the patient boundary relative to $r \geq 0$ (no correlation-constraint filtering) as a function of r-value filtering. While there is a rapid drop in image background noise even for a modest value of correlation filter ($r \geq 0.75$), there is little effect on tumor signal for $r \leq 0.90$. At $r \geq 0.90$, there is a 70% decrease, on average, in image background noise, with little or no loss of tumor signal. There is no clear correlation between diminished tumor signal with increasing r-constraint versus disease type in this small series.

Figure 3B shows the mean tumor-to-normal tissue and tumor-to-noise ratios as a function of r-value filtering. There is an initial 1.3–8.6-fold increase in tumor-to-normal tissue contrast as compared to a static 50–60-min image frame for no correlation-value filtering ($r \geq 0$), with marrow and normal breast showing the most modest average increases (1.4 and 1.3, respectively) and blood showing the most dramatic increase in contrast ratio (8.6-fold). For the range of r-value filters investigated here ($r \geq 0$ to $r \geq 0.99$), the tumor-to-normal tissue ratios increase through the entire range of correlation constraints for most tissues. The enhancements in tumor-to-normal uptake ratios are obvious.

For the patients studied here, it appears that an optimal correlation-coefficient value of $r \geq 0.90$ will produce dramatic image noise background reduction (70%) and tumor-to-normal tissue contrast ratios of 1.5–10-fold or more with little or no effect on tumor signal.

DISCUSSION

Whereas static FDG-PET imaging is a useful emerging technology, it is clear that in some patients the tumor-to-background ratios achieved are insufficiently high to detect small tumors near normal tissue with high FDG uptake (*8*). While additional delays from tracer injection until imaging may be useful in enhancing tumor-to-background ratios, such delays result in a decrease in tumor signal due to ^{18}F decay. Contrast enhancement may also be achieved by forming parametric images of the influx constant. Parametric images of the influx constant may have advantages in cancer detection over "conventional" static image analysis (typically obtained at some interval between 40 and 70 min after FDG injection) due to decreased normal tissue and blood background activity. Correlation coefficient-filtered parametric images may further reduce the normal tissue background and additionally suppress image artifacts and noise, without diminishing tumor signal. While tumor-to-background contrast is enhanced by the parametric images, a dynamic imaging sequence is required (1 hr in this study), which may lead to compromised image quality in the presence of significant patient motion. Methods for motion correction could be applied, but dynamic imaging still may prove challenging in uncooperative patients.

CONCLUSION

Enhancement of tumor-to-background contrast in PET images of cancer by the generation of pixel-by-pixel influx-constant images with an image-derived input function may provide increased detectability of tumor foci that may otherwise be obscured by residual FDG-associated activity in normal tissues and blood. An improvement to this method by "filtering" the resulting slope image by a constraint of the correlation coefficient in the linear least-squares fit has been validated. Conventional K_i images (equivalent to $r \geq 0$ filtering), while providing an improvement in tumor-to-normal tissue contrast ratio over a static FDG PET image, can lead to a noisy image containing streak artifacts. An intermediate value of correlation-coefficient filtering ($r \geq 0.90$) leads to a substantial decrease in image background noise (mean 70%) while enhancing tumor-to-normal tissue ratios over noncorrelation filtered images, with little or no decrease in the resulting tumor signal. While a correlation filter value of $r \geq 0.90$ seems optimal for the limited number of cases studied here, further clinical investigation and application is warranted to empirically determine the optimal value for an improved method of cancer detection using FDG-PET. Such studies are necessary to confirm our expectation that this methodological approach will enhance the accuracy of cancer imaging with PET.

REFERENCES

1. Choi Y, Hawkins RA, Huang SC, et al. Parametric images of myocardial metabolic rate of glucose generated from dynamic cardiac PET and 2-[^{18}F]fluoro-2-deoxy-d-glucose studies. *J Nucl Med* 1991;32:733–738.
2. Huang SC, Phelps ME, Hoffman EJ, Sideris K, Selin CJ, Kuhl DE. Noninvasive determination of local cerebral metabolic rate of glucose in man. *Am J Physiol* 1980;238:E69–E82.
3. Chen BC, Huang SC, Germano G, et al. Noninvasive quantification of hepatic arterial blood flow with nitrogen-13-ammonia and dynamic positron emission tomography [see comments]. *J Nucl Med* 1991;32:2199–2206.
4. Gambhir SS, Schwaiger M, Huang SC, et al. Simple noninvasive quantification method for measuring myocardial glucose utilization in humans employing positron emission tomography and fluorine-18-deoxyglucose. *J Nucl Med* 1989; 30:359–366.
5. Germano G, Chen BC, Huang SC, Gambhir SS, Hoffman EJ, Phelps ME. Use of the abdominal aorta for arterial input function determination in hepatic and renal PET studies [see comments]. *J Nucl Med* 1992;33:613–620.
6. Messa C, Choi Y, Hoh CK, et al. Quantification of glucose utilization in liver metastases: parametric imaging of FDG uptake with PET. *J Comput Assist Tomogr* 1992;16:684–689.
7. Zasadny KR, Wahl RL. Standardized uptake values of normal tissues at PET with

2-[fluorine-18]-fluoro-2-deoxy-D-glucose: variations with body weight and a method for correction. *Radiology* 1993;189:847–850.
8. Wahl RL, Quint LE, Greenough RL, Meyer CR, White RI, Orringer MB. Staging of mediastinal non-small cell lung cancer with FDG PET, CT, and fusion images: preliminary prospective evaluation. *Radiology* 1994;191:371–377.
9. Wahl RL, Zasadny K, Greenough R, Koeppe RA. Parametric image displays to enhance visualization of cancers with FDG-PET: influx constant and temporal subtraction imaging. *77th Scientific Assembly and Annual Meeting of the Radiological Society of North America* 1991;181(suppl):152.
10. Wahl RL, Zasadny K, Helvie M, Hutchins GD, Weber B, Cody R. Metabolic monitoring of breast cancer chemohormonotherapy using positron emission tomography: initial evaluation. *J Clin Oncol* 1993;11:2101–2111.
11. Sokoloff L, Reivich M, Kennedy C, et al. The [^{14}C]deoxyglucose method for the measurement of local cerebral glucose utilization: theory, procedure, and normal values in the conscious and anesthetized albino rat. *J Neurochem* 1977;28:897–916.
12. Weber G. Enzymology of cancer cells (second of two parts). *N Engl J Med* 1977;296:541–551.
13. Bevington PR. *Data reduction and error analysis for the physical sciences*. New York: McGraw-Hill; 1992:92–133.

Noninvasive Quantification of Iodine-123-Iomazenil SPECT

Yoshihiro Onishi, Yoshiharu Yonekura, Sadahiko Nishizawa, Fumiko Tanaka, Hidehiko Okazawa, Koichi Ishizu, Toru Fujita, Junji Konishi and Takao Mukai

Nihon Medi-Physics Co., Ltd., Nishinomiya; Fukui Medical School, Fukui; Kyoto University School of Medicine, Kyoto; and Kyoto College of Medical Technology, Kyoto, Japan

The feasibility of a noninvasive method for quantification of [^{123}I]iomazenil binding using a standardized arterial input function and a single venous blood sample was assessed in normal volunteers. **Methods:** Serial SPECT images and blood data from six healthy male volunteers after intravenous injection of [^{123}I]iomazenil were used. The standardized input function was derived by averaging the six subjects' arterial curves. Individual input functions were estimated by calibrating the standardized input function with one-point venous blood radioactivity concentration. Ligand transport (K_1) and receptor binding were computed from the estimated input functions and two separate SPECT scans using a table look-up procedure based on a three-compartment, two-parameter model. Reference values for K_1 and receptor binding were determined from the serial SPECT data and individual arterial curves using a three-compartment, three-parameter model and curve fitting. **Results:** Analyses of the error caused by the calibration in relation to the time postinjection revealed that the optimal calibration time was 30 min postinjection. Receptor binding obtained by this simplified method correlated well with the reference values ($r = 0.941$) and was estimated within an error of 10% in the cerebral cortical regions. Although the estimated K_1 showed relatively poor correlation ($r = 0.699$) with the reference value, it was an excellent relative measure in each subject. **Conclusion:** Our method provided an absolute measure of the benzodiazepine receptor binding and a relative measure of ligand transport from two SPECT scans and a venous blood sample. This method would be useful for quantitative assessment of benzodiazepine receptors in clinical settings.

Key Words: iodine-123-iomazenil; standardized arterial input function; benzodiazepine receptor; SPECT

J Nucl Med 1996; 37:374–378

Iodine-123-iomazenil is a radioiodinated ligand which has favorable characteristics for in vivo assessment of benzodiazepine receptors by SPECT: high brain uptake, little nonspecific binding, high affinity for benzodiazepine receptors and no intrinsic pharmacological effects at tracer doses (*1–6*). Various SPECT studies have demonstrated the clinical feasibility of [^{123}I]iomazenil for the assessment of benzodiazepine receptors in the living human brain (*7–12*).

Brain tissue distribution of [^{123}I]iomazenil is determined by at least two independent factors, i.e., the ligand transport and the binding characteristics of the receptors. Consequently, SPECT image counts depend not only on the characteristics of the benzodiazepine receptors but also on regional cerebral blood flow, even though imaging is performed at an appropriate time after injection of the radioactive ligand. These two factors can be determined separately with SPECT or PET by using compartmental analysis (*13–19*). Quantification requirements, such as rapid serial data acquisition over a long time period and frequent arterial blood sampling, are too laborious for routine clinical practice.

Since [^{123}I]iomazenil can be used in many nuclear medicine facilities with SPECT, a noninvasive method for quantitative measurement of receptor binding would have significant clinical value. We recently demonstrated that quantification of the ligand transport and benzodiazepine receptor binding of [^{123}I]iomazenil can be achieved with two separate SPECT scans using a three-compartment, two-parameter model and a table look-up procedure (*16*). Application of such quantitative measurement would become possible in routine clinical studies if arterial blood sampling were not necessary. In this study, we used data obtained in normal volunteers to assess the precision of measures of receptor binding and ligand transport of [^{123}I]iomazenil with a single venous blood sample instead of frequent arterial blood sampling, using the concept of standardized arterial input function (*20–22*).

METHODS

Subjects

Serial SPECT images and blood data obtained in our facility for six healthy male volunteers (aged 24–61 yr; weight: 53–79 kg) after an intravenous bolus injection of 111 MBq [^{123}I]iomazenil were used (*16*). The data were acquired and processed as follows.

Blood Data. Arterial blood samples (1–3 ml) were drawn through a radial artery catheter at 5-sec intervals for the first 40 sec and subsequently at 50 sec and 1, 1.5, 2, 3, 5, 10, 20, 30, 60 and 120 min postinjection. Total radioactivity concentrations in the whole blood and plasma were measured. The lipophilic radioactivity concentration in arterial plasma was determined by chloroform extraction, followed by washing of the organic layer with saline to minimize contamination by hydrophilic metabolites (*16*). Venous blood samples were drawn at 3, 5, 10, 20, 30, 60 and 120 min after

Received Dec. 29, 1994; revision accepted Jul. 30, 1995.
For correspondence or reprints contact: Yoshihiro Onishi, Nihon Medi-Physics Co., Ltd., 9-8 Rokutanji-cho, Nishinomiya 662, Japan.